DOI: 10.13009/EUCASS2022-6357
9TH EUROPEAN CONFERENCE FOR AERONAUTICS AND SPACE SCIENCES (EUCASS)

Novel Morphing High-Lift Devices for Laminar Wing Design of Turboprop Aircraft – Large-Scale Wind-Tunnel and CFD Assessment

Stefan Wallin[1], Ardeshir Hanifi[1], Stephan Adden[2], Francesco Amoroso[3] and Faranggis Bagheri[4]
[1] KTH, FLOW Turbulence Lab
Dept. Engineering Mechanics, KTH, SE-100 44 Stockholm, Sweden
[2] IBK Innovation GmbH
Butendeichsweg 2, 21129 Hamburg, Germany
[3] Eurotech SAS
Via L. Paestum 239, 84047 Capaccio Paestum (SA), Italy
[4] neptech AB
Kyrkogårdsvägen 137, 121 34 Enskededalen, Stockholm, Sweden

Abstract
A previous large-scale wind tunnel model of a turboprop aircraft for regional transport has been redesigned to utilise natural laminar flow. The 1:6.5 scale model is a complete aircraft with running and thrusting propellers and all the essential aerodynamic control surfaces can be set at different positions. The performance of innovative high-lift configurations by the use of morphing technology has been evaluated for cruise, take-off and landing configurations where both the leading edge and trailing-edge flap are drooped. The model was equipped with two different wing designs with corresponding high-lift configurations. A wind-tunnel campaign took place at RUAG, Emmen, where both wing designs were measured for the different high-lift configurations including control surface settings and engine thrust variations. The extensive experimental data set was complemented by CFD analysis for extrapolation to free-flight full-scale conditions. Moreover, wind-tunnel installation effects, turbulence modelling and transition to turbulence were studied by CFD, which also provided additional understanding of the complex three-dimensional flow field.

1. Introduction

Regional mobility in terms of air transportation is of fundamental importance for regional economic and social development by connecting countries, people and cultures. In this respect, novel turboprop designs will contribute to environmentally friendly and sustainable means of transportation. Turboprop configurations are efficient providing fuel savings of up to 20 percent with respect to equivalent technology turbofan aircrafts [1], and novel propeller design enables cruise speeds up to Mach 0.8, see e.g. [2] and [3].

Moreover, additional drag reduction can be achieved by utilizing natural laminar wing technology by imposing a favorable pressure gradient on a large part of the upper wing surface which will accelerate and stabilize the boundary layer. This would pose particular requirements on the particularly shaped upper surface requiring smooth and continuous flow which will disqualify traditional high-lift devices such as slotted leading-edge flaps. Introducing flexible leading-edge structures which can be drooped during take-off and landing has been suggested, see e.g. [4] and [5].

The integration of turboprop engines into the airframe, and the design of high-lift devices for landing and take-off, presenting some unique aerodynamic challenges in particular when utilizing natural laminar flow wings for additional drag reduction. These issues were addressed within the Clean Sky 2 project WTM-RECYCLE, completed during 2021, supporting the development and assessment of new and conceptual versatile aerodynamic high lift technologies as well as turboprop integration effects.

DOI: 10.13009/EUCASS2022-6357

Previous research projects funded by the European Union through the CleanSky and CleanSky 2 Research Programmes related to an innovative regional turboprop aircraft have been performed including wind tunnel measurements of a 5m span large-scale turboprop aircraft model, the LOSITA model [6]. The previous LOSITA model had thrusting innovative turbo-prop propellers, but with a more traditional wing design with leading-edge slat and trailing-edge flap high-lift devices.

In the present work, the LOSITA model will be recycled and redesigned with the focus on the wing design and high-lift devices introducing drooping technology for enabling natural laminar flow. Wind tunnel measurements of a 5m span large-scale turboprop aircraft model together with complementary CFD analyses were used to study the effect of morphing devices for drooped wing leading edge, geometry morphed flaps and winglets. Two different wing profile geometries in cruise, landing and take-off configurations were studied. Propeller installation effects were included by powered thrusting propellers in the wind-tunnel installation as well as in the CFD model. The paper will present the redesign and manufacturing of the model, the wind-tunnel test campaign at RUAG, as well as the complementary CFD study.

2. Model redesign and manufacturing

The projects objectives were to design a wind-tunnel model from an existing baseline solution that makes use of the modularity and thus allows using the mentioned for a large number of different configurations. Different configuration in this sense means that at first the wing itself has various configurations (LE-devices, TE-devices, Wing-tip) but second also means the implemented wing can be replaced by a completely different wing with minimum effort during a running test-campaign, allowing as well for the second wing to be tested with various different configurations.
The WT-model itself consists of the following features:

- turboprop-engine simulator realized via hydraulic motor
- movable/adjustable leading edge and trailing edge devices
- adjustable wing-tip device
- movable elevator and rudder
- two wings
    - LND, Leonardo-Wing based on a wing-profile defined by Leonardo
    - NLF-Wing based on a wing-layout developed in the frame of Cleansky

All movables were targeted to be set to specific, pre-described conditions.
With regard to instrumentation the Wind-Tunnel provided a six-component balance for measuring all forces and moments. Additionally, pressure-tabs were introduced in all wings, HTP and VTP. The model mounted with the vertical sting can be seen in Figure 1.

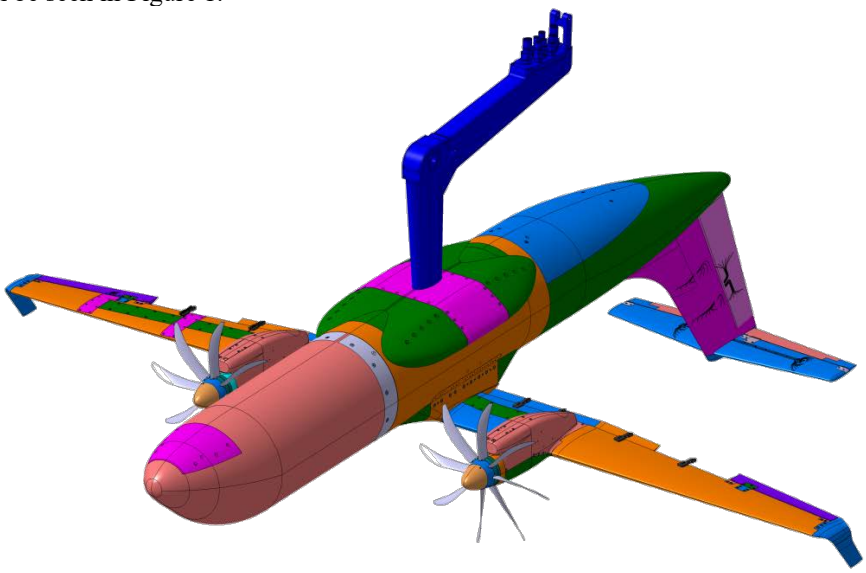

Figure 1: WT-Model tested during the project WTM-RECYCLE (Leonardo-wing).

DOI: 10.13009/EUCASS2022-6357

Exchanging large items during a WT-test campaign usually reduces the overall performance of the campaign. In order to conduct a large number of polars configuration-changes should be optimized in a way that they are limited as much as possible. Changes taking a long lead time are not favorable.

In the current project the design performed by IBK therefore contains smart solutions to enable changing the wings within the test-campaign with minimum effort. This is particularly difficult due to the fact that both wings have running engines-mounted to them. These engines are operated with oil-hydraulics (up to 400 bar) provided by the WT. Ensuring the tightness of the oil-transporting system is a difficult job that requires careful tests during the WT-installation. Doing this in a running test-campaign due to a major configuration change is not advisable and poses a strong risk for the test-campaign. Thus, a design solution has to be found that is addressing this issue. To comply with this need, the wing mounting solution from the previous WT-model could not be kept and had to be redesigned. The core design idea to successfully address this topic therefore was to ensure that the wing was designed with a central core-wing and additional, external mounted covers to comply with both aerodynamic shapes. Designing the wing like this the core wing, including the hydraulics, can be kept during the campaign, and only the outer wing elements need to be swapped. Figure 2 shows this design approach.

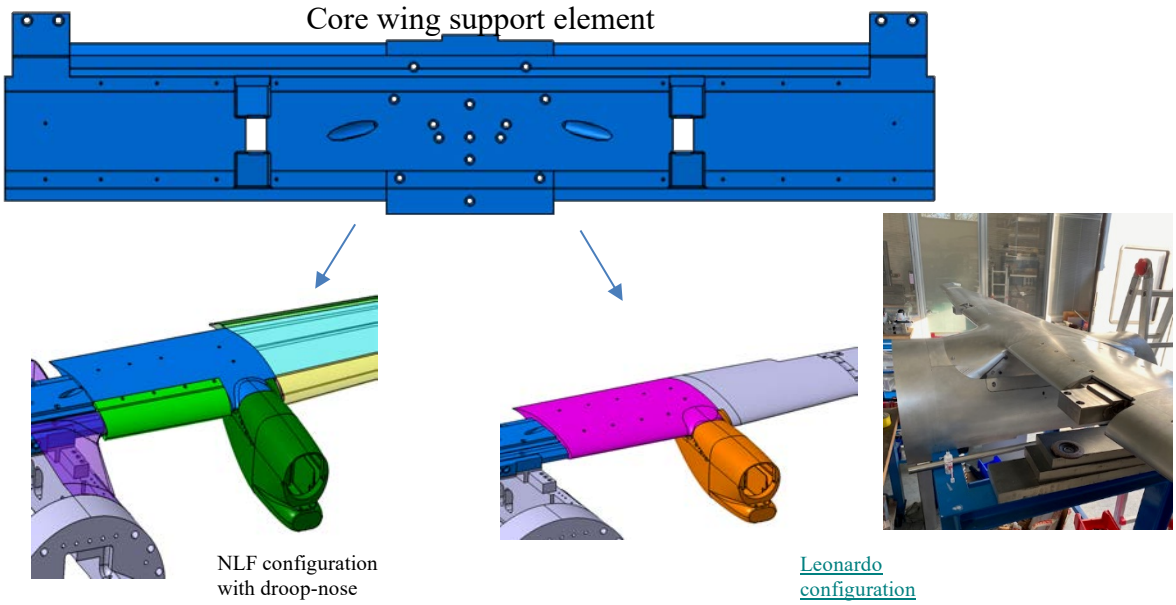

Figure 2: Design solution for modular wing.

In both cases an outboard wing was designed (for Leonardo configuration already available from previous test-campaign) that was mounted to the core wing support element. The outer wing as well as the panels mounted to the core wing support element are instrumented, therefore parallel to the mechanical connection quick connectors were used to efficiently adapt the pneumatic connection.

The most critical element of this campaign therefore is the core wing support element; therefore the focus of this design chapter stays on this item. It needs to address several purposes:

- enable mechanical connection to the fuselage
- hydraulic routing of oil to left and right wing engines
- mechanical connection of two different outboard wings
- mechanical connection of panels to create both wing-shapes
- pneumatic routing of outboard wing pressure tabs
- quick and efficient pneumatic connection of inboard pressure tabs mounted on panels

The final solution of this part can be seen in more detail in Figure 3.

DOI: 10.13009/EUCASS2022-6357

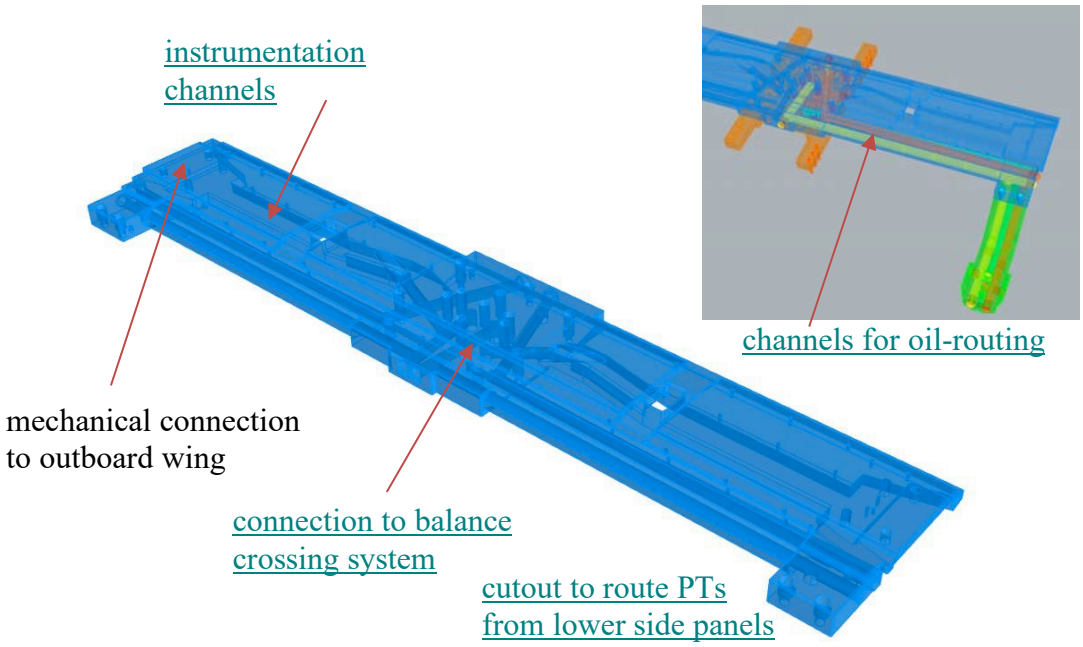

Figure 3: Detailed solution for core wing support element.

The final solution resulted in very complex part, which was mainly created by milling. The oil-routing lines were drilled, a specific long drill was used to create these large holes. In particular the interface to the already existing balance/ balance crossing system was complex and results in a complex local milling/ drilling solution.

The model manufacturing and assembly as well as the mounting support in the WT was performed by the company EUROTECH.

3. Experimental campaign

The test was performed in the LWTE in Emmen, Switzerland, operated by RUAG in 2021. In total 400 polars were tested. Due to priorities of test-activities, in total ~310 polars were spent on the Leonardo setup while ~90 polars were used for the NLF-setup. In both configurations landing, takeoff and cruise settings were applied.
The breakdown is as follow:
Leonardo-Configuration:155 polars with engines running (full, one-engine out, feathered prop)

- 37 Landing-Polars
- 62 Takeoff-Polars
- 56 Cruise-Polars

Leonardo-Configuration: 154 polars with engines not running (no-blade setup)

- 81 Cruise-Polars
- 43 Landing-Polars
- 30 Takeoff-Polars

NLF-Setup: 91 polars with engines not running (no-blade setup)

- 58 Cruise-Polars
- 15 Landing-Polars
- 18 Takeoff-Polars

Parameter to be varied during the polars were mainly aileron, rudder and HTP setting for each of the individual flight-configurations. The Leonardo-configuration was tested engine-on and engine-off, the NLF configuration only with engine-off. The configurational change from Leonardo-configuration to NLF-configuration was established in within the expected timeframe for this change, thus showing that the overall design approach was feasible. A very big obstacle in this test-campaign was the remote-attendance of all partners due to the COVID-19 situation in Europe. It can be clearly said that this resulted in a difficult way of communicating in particular when issues/questions during the

DOI: 10.13009/EUCASS2022-6357

campaign required feedback from either model-design (IBK), model manufacturing (EUROTECH) or test-prioritizing (Leonardo).

The test itself were successfully conducted, thanks to a very strong effort taken by RUAG in particular due to the problems around the lacking personal attendance of the partners. RUAG established online monitoring of the test including video links as well as direct access to the test data base for the project team. The test-results will be shown in more details in the following chapter, in which the comparison of the various configuration with CFD-methods can be seen. Due to the large amount of data only parts of the results can be shown here.

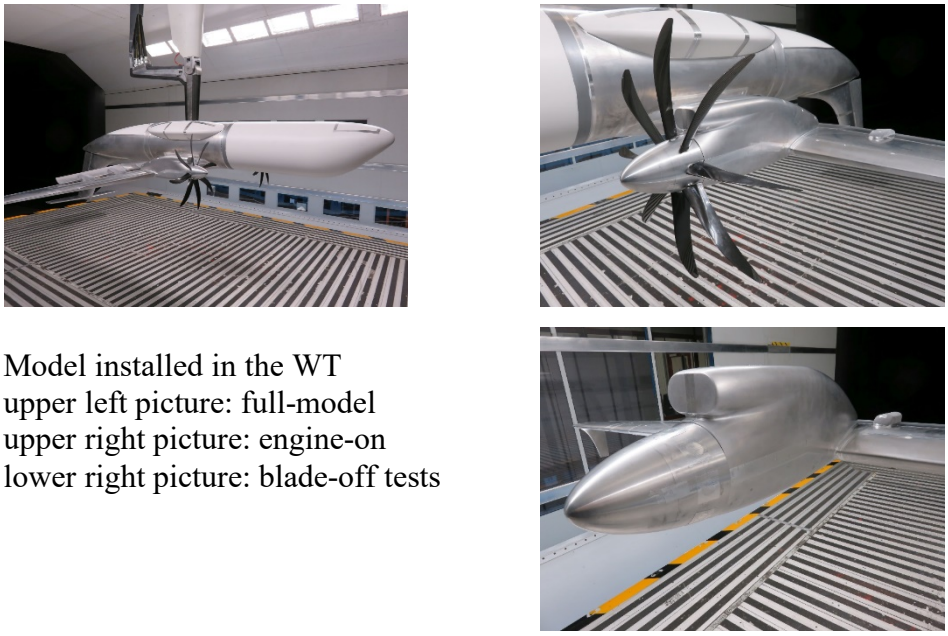

Figure 4: Figures of the model in the WT with different setups.

4. CFD study

4.1 Meshing and geometry

The CFD model reproduces the wind-tunnel model in most aspects. The complete aircraft is modelled including fuselage, tail, wing with high-lift devices, winglet, engine pylon and nacelle as well as running and thrusting propellers. Since the propellers are co-rotating, the flow over the left and right wings will not be symmetric and a full model must be realized.

Both wing designs, LND and NLF, will be included in the CFD study. Moreover, both wings will be configured for cruise, take-off and landing. A drooped geometry for the leading edge is imposed at take-off and landing conditions while the trailing-edge flap is drooped only for the landing configuration, see Figure 5. The full aircraft geometry becomes fairly complex with details around the wing-fuselage and wing-pylon interfaces being dependent on the different wings and settings.

The meshing strategy for the most efficient CFD results in terms of required resolution for a certain accuracy is to generate quad dominated (structured) surface meshes over the smooth regions of the geometry. These are the fuselage, tail and a large part of the wings and trailing-edge flaps. The wing and flap leading edge curvature radii are small in comparison with the span and a structured surface mesh around these, where high-aspect ratio surface cells are allowed, is of particular important for efficient resolution. High quality boundary-layer meshing is then generated by extruding the surface mesh into the flow domain.

Such high-quality meshing cannot be completely facilitated by automatic meshing procedures, and some amount of manual building is necessary. However. the different details of the wings and aerodynamic surfaces must be easily interchangeable within the CFD model for enabling rapid turn-around times for the CFD study. For these reasons, the

DOI: 10.13009/EUCASS2022-6357

strategy taken for building the CFD model is to a large extent the same as for building the physical wind-tunnel model. Each part of the CFD model is carefully designed with defined interfaces and meshed independently by carefully designing high-quality boundary-layer meshes based on structured surface meshes. Each part would of case require some amount of manual work, but the number of components are very much reduced in comparison with the number of combinations that are needed in the parameter study. The different parts can then be automatically combined through a master meshing script. Moreover, for all different settings there is the option of far-field free-stream conditions or introducing the wind-tunnel walls as slip walls with identical near-field meshing. The resulting surface mesh for one high-lift configuration is illustrated in Figure 6.

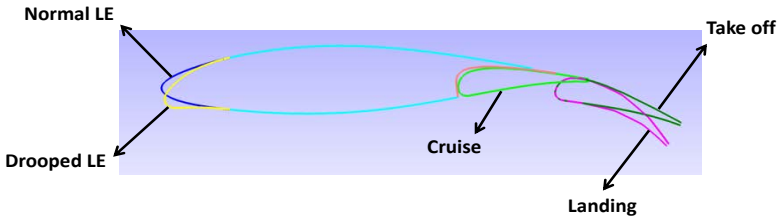

Figure 5: The different configurations used for the CFD study for both wing designs shown as profiles trough the inboard wing section.

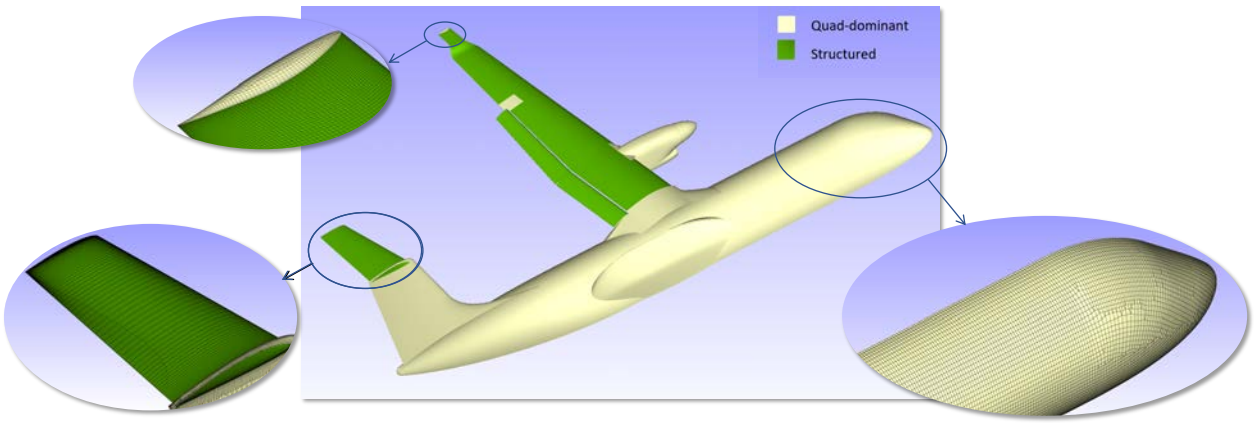

Figure 6: Illustration of the surface mesh where the green parts are regular structured surface patches and the greay parts are the remaining surfaces, which are quad-dominant automatically generated.

4.2 CFD setup and baseline comparisons

The CFD solution is obtained by utilizing the M-Edge general-purpose finite volume flow solver, applicable for both structured and unstructured grids [7]. The governing equations are integrated to steady state using an explicit multistage Runge-Kutta time integrator combined with a line-implicit approach [8] for convergence acceleration for stretched grids. Low-speed preconditioning is used mainly for higher numerical accuracy. Weak formulations for the boundary conditions are used [9].

The turbulence is modelled, aiming for a steady-state Reynolds averaged Navier-Stokes (RANS) solution, by the use of two different models. The Wallin & Johansson explicit algebraic Reynolds-stress model (EARSM) [11] together with the Hellsten [10] k-ω two-equation model is able to capture some effects of strong three-dimensionality such as swirl and corner flow separation, e.g. related to wing-body and wing-pylon interactions. Comparison is made with the Spalart-Allmaras (S-A) one-equation model [12], which is highly tuned and optimized for aerodynamic applications.

The experimental campaign was performed at the very last few months in the project and, hence, most of the CFD results were produced before the experimental data was available. The primary aerodynamic quantities are shown in Figure 7 where the experimental data is compared with CFD. In general, the comparison is good within the linear regime of AoAs, up to 10 to 15 degrees. The figure shows the results for the LND wing design at cruise, landing and take-off. The results for the NLF configurations are quite similar and will not be elaborated upon here and are not shown. The EARSM predicted premature stall for the high-lift configurations, though. The reason for that is not clear, but it can be related to some differences in the geometrical details not captured in the CFD model such as the flap

DOI: 10.13009/EUCASS2022-6357

fairings. The acceleration of the flow in between these contractions and the related stream-wise vortices may promote attached flow over the flap where the CFD model indicates separated flow.

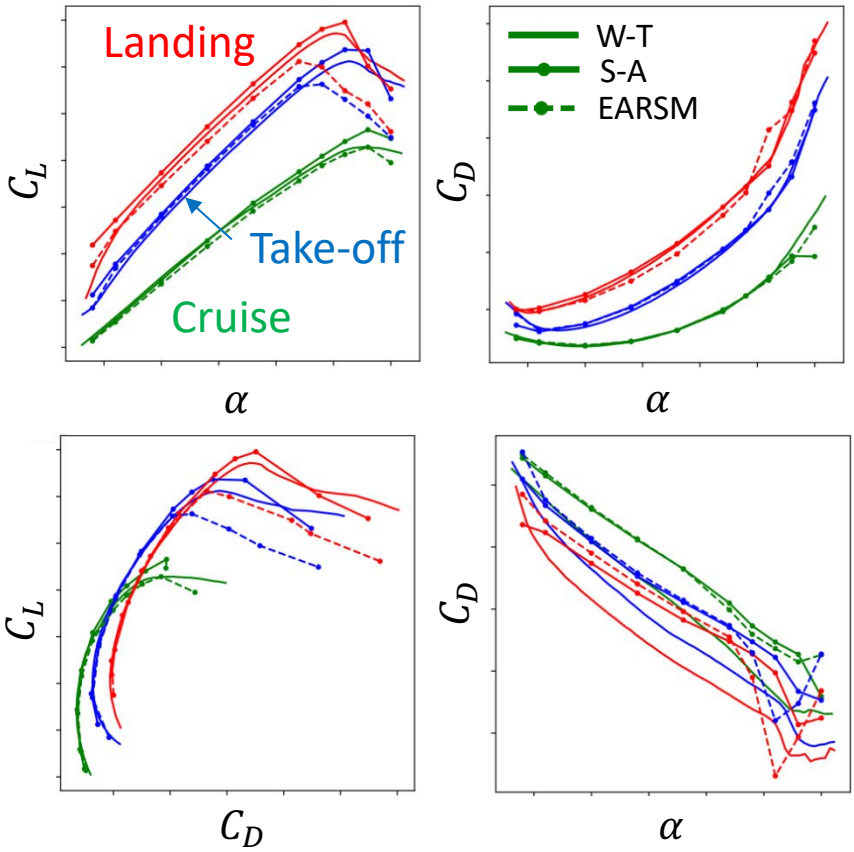

Figure 7: Aerodynamic performance for the LND wing design at Cruise, Take-off and Landing. CFD results using EARSM and Spalart-Allmaras RANS models are compared with force measurements.

There is an offset in pitching moment between the CFD and experimental results where the CFD is overpredicting Cm by around 0.2. We have no clear explanation for this. The offset would correspond to about 3 deg in the elevator setting, but the accuracy in the experimental setup is much higher than that.

The surface pressure distribution over the inboard NLF wing at y=-0.4 is shown in Figure 8 for cruise and Figure 9 for takeoff and landing configurations. The pressure distribution is in general better captured by the EARSM model than by the Spalart-Allmaras model except for the high-lift post-stall AoAs. This might be seen as another indication of that the premature separation seen for EARSM is not related to the flow over the wing, but rather on the separation over the flap.

Finally, Figure 10 illustrates the separated flow over the NLF wing design at take-off. The oil-flow visualisation for AoA=14 deg shows a flow pattern with high complexity. We can see the trace of the nacelle vortices and the wing-body junction separation. Also the initial trailing-edge separation at the outer part of the outboard wing is seen, where the drooped leading edge and flaps are not protecting the flow. All these features are well predicted by the CFD model but with somewhat different amplitudes and somewhat different AoAs between 14 and 16 degrees. The illustration also shows that the traces of the flap fairings are absent in the CFD but visible in the oil-flow picture.

DOI: 10.13009/EUCASS2022-6357

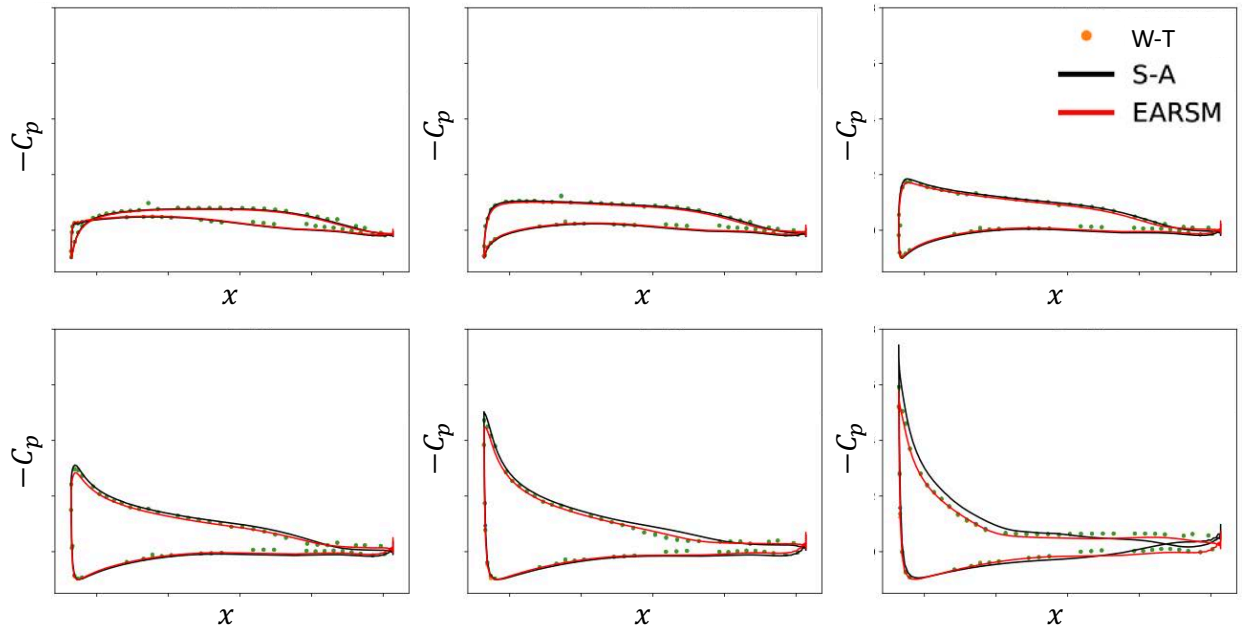

Figure 8: Surface pressure over the inboard main wing for the LND wing design at Cruise for different AoA (0, 4, 8, 12, 16, 20 deg.). CFD results using EARSM and Spalart-Allmaras RANS models are compared with pressure tap measurements.

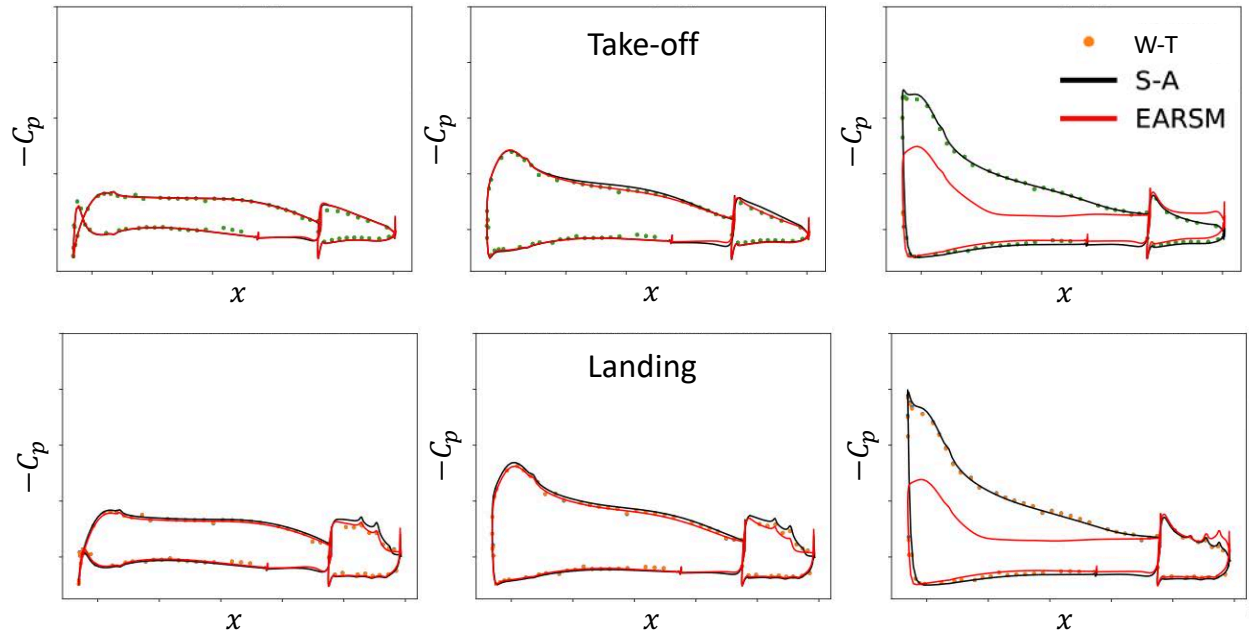

Figure 9: Surface pressure over the inboard main wing for the LND wing design at Take-off (top) and Landing (bottom) for different AoA (0, 8, 16 deg.). CFD results using EARSM and Spalart-Allmaras RANS models are compared with pressure tap measurements.

DOI: 10.13009/EUCASS2022-6357

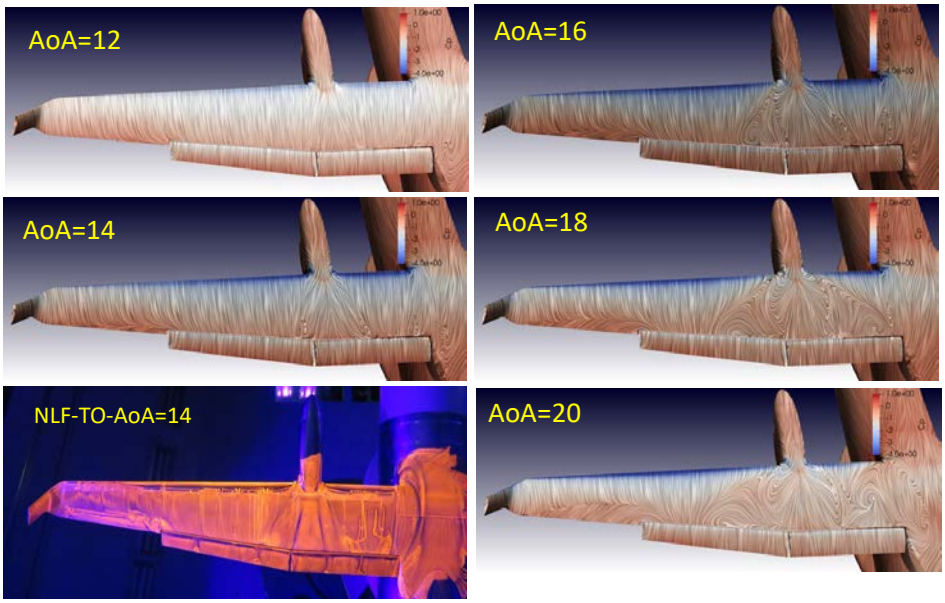

Figure 10: Skin friction lines derived from CFD at a range of AoAs, in comparison with experimental oil-flow patterns at AoA=14 deg for the NLF wing design at Take-off.

4.3 Propeller actuator disk model

A propeller model is used in the CFD model for representing the thrusting propellers in the wind-tunnel experiment. An actuator disk model [13] provides thrust and swirl based on the local flow conditions and local blade data. The propeller geometrical data given as chord and twist v.s. radius is in accordance with the propeller used in the experiments. The blade pitch angle in the CFD model is calibrated for a thrust coefficient TC=0, 0.1 and 0.2 by using the actuator disk model mounted on a hub in free stream, Figure 11 left. The TC is then verified for the same actuator disk model and settings installed at the model aircraft, Figure 11 right, confirming values close to the ideal free-stream ones. In this figure the asymmetry induced from the co-rotating propellers are clearly seen. The TC is defined as the thrust normalized as the lift and drag coefficients are. The procedure of calibrating the blade pitch angle is the same as used for the experimental setup and the resulting pitch angles compares well between the CFD and experimental calibration. The low-speed preconditioning used is crucial for obtaining the sharp propeller slip stream clearly shown in the left figure for the free-stream case.

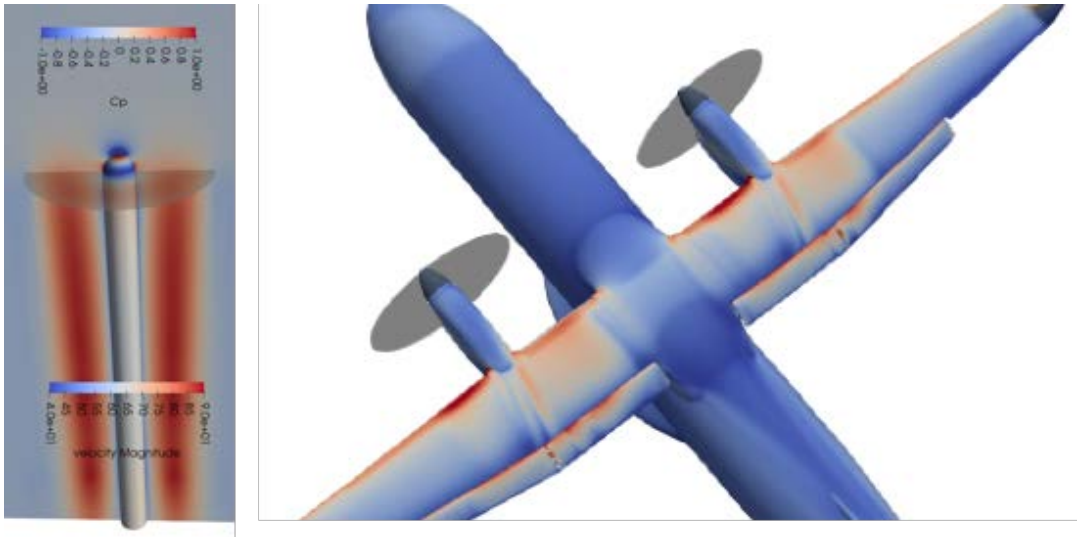

Figure 11: Illustration of the calibration of the propeller actuator disk model. Isolated propeller in free flight (left) and installed on the aircraft model (right).

DOI: 10.13009/EUCASS2022-6357

Figure 12 shows the influence of the thrusting propellers. There are some convergence problems related to the propeller disk model for higher AoAs so values for AoA>10 should not be considered as representative. In general, for lower AoAs, the influence of the thrusting propeller compares well with measurements. The surface pressure distribution at AoA=8 shows that EARSM is able to capture the interaction with the propeller slip stream on the leading edge much more accurate than the Spalart-Allmaras model.

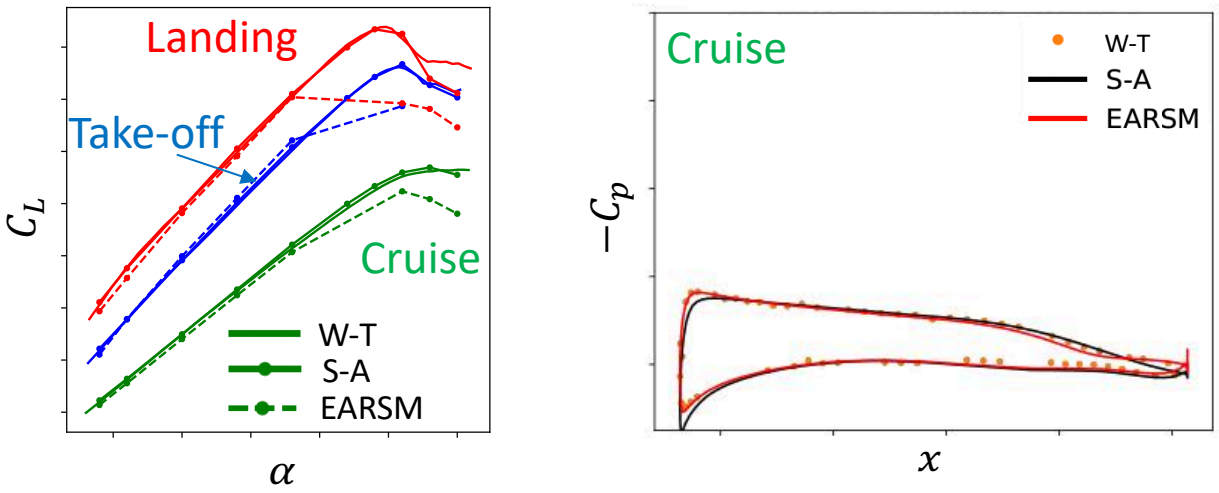

Figure 12: Computed lift polar (left) for thrusting propellers with TC=0.1 for the LND wing design. Corresponding surface Cp distribution (right) for Cruise condition at AoA=8 over the inboard wing (y=-0.4m).

4.4 Wind-tunnel interference, extrapolation to free flight and turbulence transition

The influence of the wind-tunnel walls is estimated through the wind-tunnel corrections when extrapolating the wind-tunnel measurements to free-stream conditions. In the CFD framework the wind-tunnel installation effects can be quantified by computations where the wind-tunnel walls are present (see Figure 13) and compare with free-stream computations. The wind-tunnel walls are implemented as slip walls to avoid the need of resolving the wind-tunnel wall boundary layers. While the AoA can be set from the direction of the incoming velocity in free-stream conditions, each AoA needs to be meshed independently when the wind-tunnel walls are present. For best comparison, most accurate delta effects, the near-field mesh is kept fixed and constant for all cases with and w/o wind-tunnel walls and only the far field is remeshed. This will also reduce the turn-around time for generating all wind-tunnel meshes for different AoAs.

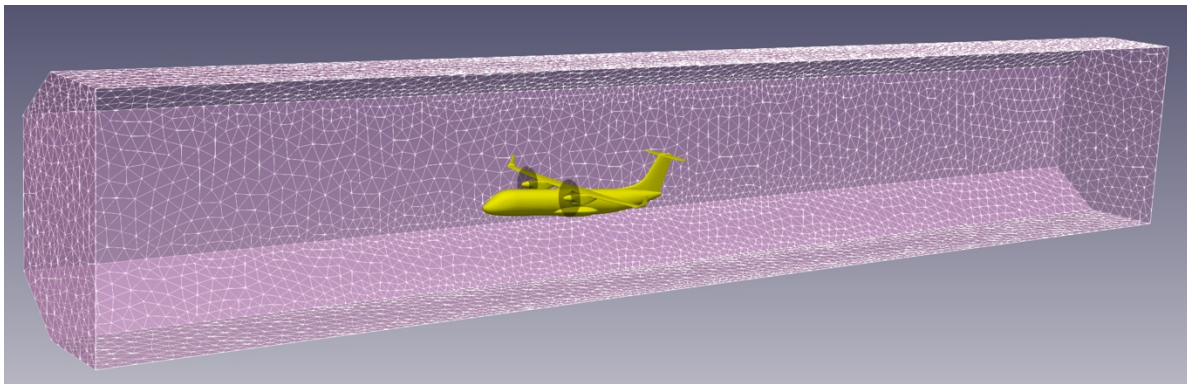

Figure 13: CFD model enclosed by wind-tunnel walls.

Figure 14 shows the computed difference between free-flight and wind-tunnel conditions. Obviously, no wind-tunnel measurements for free-stream conditions can be obtained, but the uncorrected and corrected wind-tunnel data is used for representing the wind-tunnel and free-flight conditions respectively. In fact, this study is then comparing the CFD computed wind-tunnel corrections with the established ones used for the RUAG facility. Although, the absolute values

DOI: 10.13009/EUCASS2022-6357

of lift are somewhat off, the wind-tunnel installation delta effects computed by CFD compare well with the established wind-tunnel corrections. The wind-tunnel interference is larger for the landing configuration compared with cruise condition due to the higher induced lift and far-field circulation, which is captured both in the CFD results and by the wind-tunnel correction. If the consistent comparison is verifying the accuracy of the CFD results or the wind-tunnel corrections is up to the reader to judge.

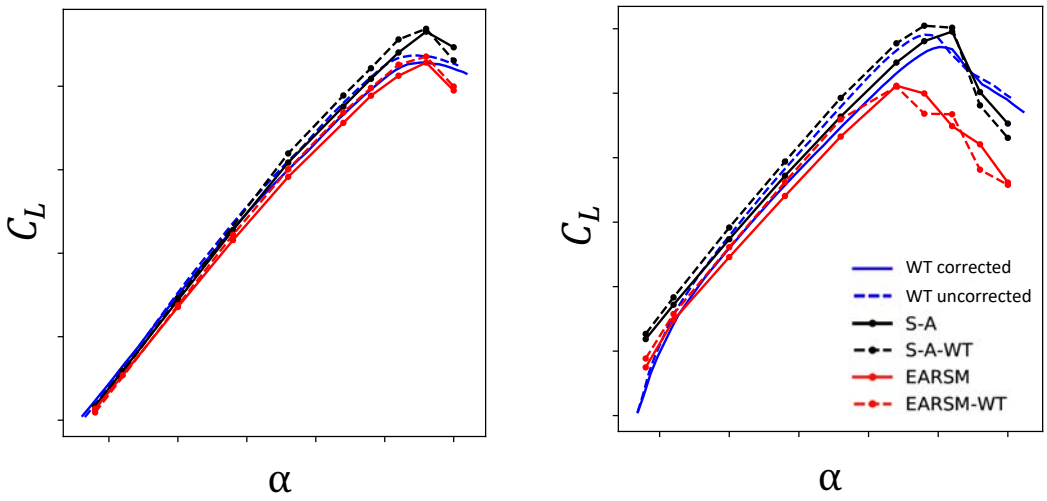

Figure 14: Computed lift polar in cruise (left) and landing (right) conditions comparing wind-tunnel installation effects. Free-flight CFD is compared with corrected WT data and CFD with wind-tunnel walls is compared with uncorrected WT data.

Further, CFD can provide an estimate of the influence of extrapolation to full-scale conditions without the limitations imposed by the wind-tunnel performance. The increased Reynolds number (Re) in full scale conditions would pose additional requirements on the computational mesh near-wall resolution for keeping the wall y+ values around unity. However, in this study, we are able to keep the same mesh also for the higher Re resulting in y+ around 5 by applying an improved universal wall boundary condition [15], which is a further development of [14]. The delta effects will then be free from any influences of differences in meshing. The influence of the increased Re for full-scale conditions is shown in Figure 15. As expected, the lift increases for higher AoAs and drag decreased for all AoAs.

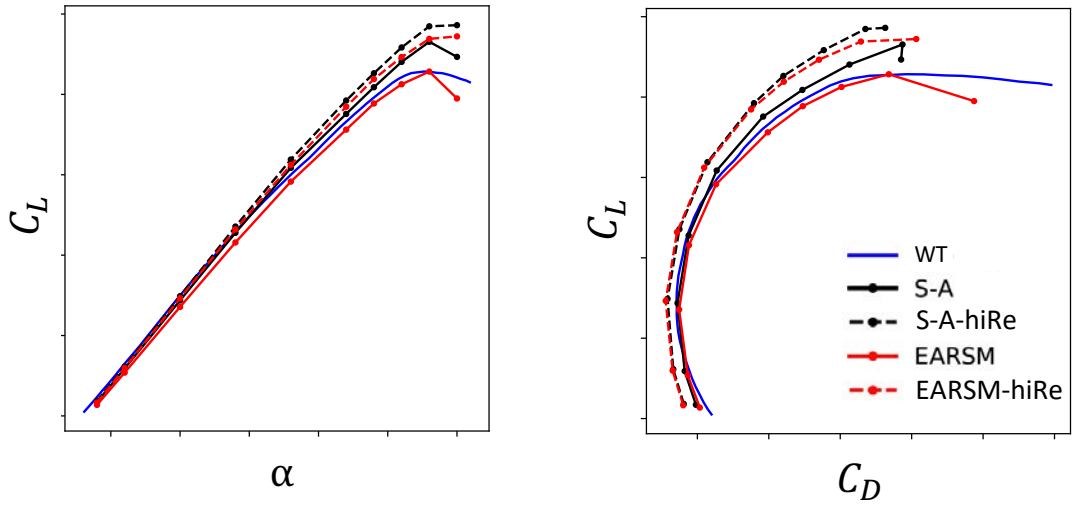

Figure 15: Computed lift (left) and drag (right) polars for wind-tunnel and full-scale (hiRe) Reynolds numbers for the LND wing design and Cruise configuration.

Transition is predicted by applying the e^N method using the procedure [17]. The pressure distribution is extracted at 27 spanwise positions over the wing and is used for computation of the laminar boundary layer profiles. The ONERA

DOI: 10.13009/EUCASS2022-6357

database method [16] is used for estimating the growth rate of TS-waves and cross-flow vortices. The transition point was predicted to be where the amplification factor has reached $\exp(N_{Tr})$. N_{Tr} = 5.4 and 9 is used for wind-tunnel and free-flight conditions respectively. The quasi-structured meshing around the wing leading edge results in smooth pressure distributions that can be used directly without smoothing for the boundary-layer computations. Both wing designs have been analysed in cruise conditions for AoA=4 and in high-lift conditions for AoA=8. Figure 16 shows the skin friction for the LND wing design in cruise for wind-tunnel and full-scale free-flight conditions. The transition is predicted to be later for the higher Re, which is somewhat surprising, but this is due to the higher disturbance levels in typical wind-tunnel conditions (different N_{Tr} values). The NLF wing design shows similar results.

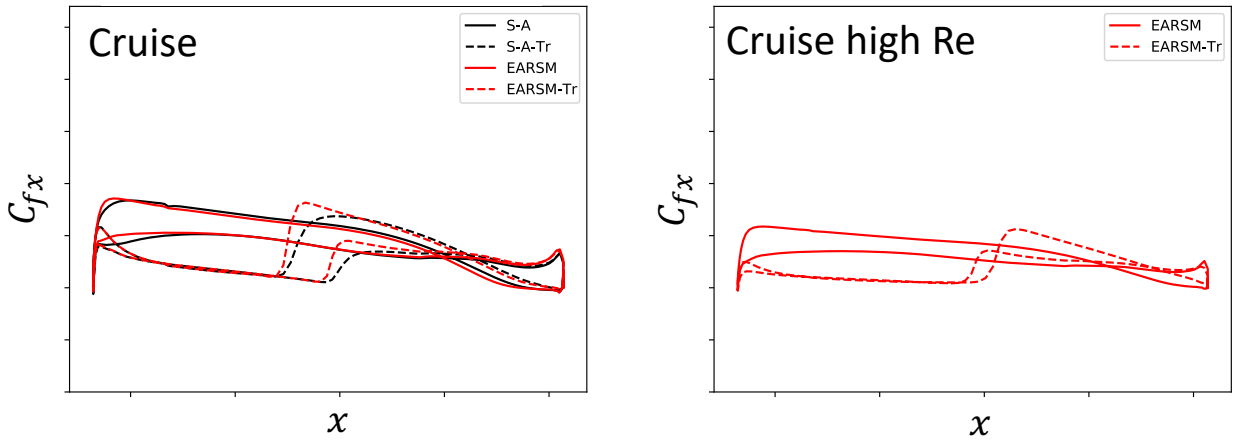

Figure 16: Computed skin friction coefficient assuming fully turbulent and with transition predicted for the LND wing design in Cruise conditions at wind-tunnel (left) and full-scale (right) Reynolds numbers.

5. Concluding remarks

The WTM-RECYCLE was an ambitious project with several different novel concepts, not only related to the innovative aircraft design, but also related to the methodology, which is the focus of the present paper.

The wind-tunnel model is a large-scale 5m span complete aircraft with running and thrusting propellers including fuselage and tail. All essential aerodynamic control surfaces such as ailerons, inner and outer spoilers, rudder and elevator are included and can be set in different positions. Moreover, cruise conditions as well as landing and take-off configurations are set by interchangeable parts. All these settings must be easily and accurately made for rapid turn-around times during the wind-tunnel campaign and for good repeatability. Moreover, the high-lift configuration changes must be rapidly and easily made as well with high repeatability including connections to instrumentation such as pressure taps and flap balances.

However, the biggest challenge was that two different and interchangeable wing designs were included in the test campaign with the wing change made during the test campaign within the wind tunnel. The two wings have different aerofoil profiles and, hence, different high-lift designs and fairings connecting the fuselage and engine pylon. The smart design and careful manufacturing of the parts enabled us to complete the wing change within a few hours inside of the wind tunnel. The engines were fed by a high-pressure hydraulic system that was kept untouched during the wing change to avoid oil leakage and the need for additional pressure tests.

CFD analysis was included in the project as well with the main purpose of complementing the wind-tunnel measurements with extrapolation to free flight and to full-size Reynolds number as well as providing deeper understanding of the flow-field, stall processes and wind-tunnel installation effects. Hence, the aim with the CFD study was not (only) to validate the CFD methods.

The CFD model was built in parallel with the hard-ware design with similar methodology of carefully designed and manufactured (in terms of computational mesh) interchangeable parts for rapid turn-around times. This is, to some extent, a novel concept in contrary to more automatic meshing procedures directly based on the geometry with lesser possibilities to design high-quality meshes. Most of the CFD analyses were obtained blindly before the test results were available.

DOI: 10.13009/EUCASS2022-6357

In conclusion, interesting and useful results were produced from the project with a massive amount of wind-tunnel data and complementary CFD data.

Acknowledgements

The study was performed within the project WTM-RECYCLE, which received funding from the Clean Sky 2 Joint Undertaking under the European Union's Horizon 2020 research and innovation programme under grant agreement No 755605. Computational resources were provided by the Swedish National Infrastructure for Computing (SNIC). The authors sincerely acknowledge RUAG and Eurotech personnel for their essential support during the experimental campaign.

References

[1] Dugan, J.F., Bencze, D.P. and Williams, L.J. 1977. Advanced turboprop technology development. In proceedings of *Aircraft Systems and Technology Meeting*, Seattle, WA, USA.

[2] Kong, C., Park, H., Lee K. and Choi, W. 2012. A Study on structural design and analysis of composite propeller blade of turboprop for high efficiency and light weight. In proceedings of *ECCM15—15th European Conference on Composite Materials*, Italy.

[3] Aschwanden, P., Mueller, J., Griiths, R., Smith, B. and Northall, R. 2012. Wind tunnel testing of a counter rotating open fan powered aircraft configuration. In proceedings of *28th Aerodynamic Measurement Technology, Ground Testing, and Flight Testing Conferenc*e, New Orleans, Louisiana. https ://doi.org/10.2514/6.2012-2860.

[4] Monner, H. P., Kintscher, M., Lorkowski, T. and Storm, S. 2009. Design of a smart droop nose as leading edge high lift system for transportation aircrafts. In proceedings of *50th AIAA/ASME/ASCE/AHS/ASC Structures, Structural Dynamics, and Materials Conference*, Palm Springs, CA, USA.

[5] De Gaspari, A., Gilardelli, A., Ricci, S., Airoldi, A. and Moens, F. 2018. Design of a leading edge morphing based on compliant structures for a twin-prop regional aircraft. In proceedings of *2018 AIAA/AHS Adaptive Structures Conference, AIAA SciTech Forum*, Kissimmee, FL, USA.

[6] Centracchio, F., Averardo, M., Di Giulio, M., Gemma, R., Pelizzari, E., Adden, S., Aschwanden, P., Müller, J., Berkefeld, T., Haxter, S. and Amoroso, F. 2020. Aerodynamic and aeroacoustic investigation of an innovative regional turboprop scaled model: numerical simulations and experiments. *CEAS Aeronaut J* **11,** pp. 575–590. https://doi-org.focus.lib.kth.se/10.1007/s13272-020-00437-y.

[7] Eliasson, P. and Weinerfelt, P. 2007. Recent Applications of the Flow Solver Edge, In proceedings of 7th Asian CFD Conference, Bangalore, India.

[8] Eliasson, P., Nordström, J., and Weinerfelt, P. 2009. Application of a line-implicit scheme on stretched unstructured grids. In 47th AIAA Aerospace Sciences Meeting Including the New Horizons Forum and Aerospace Exposition, AIAA 2009-163.

[9] Nordström, J., Eriksson, S. and Eliasson, P. 2012. Weak and Strong Wall Boundary Procedures and Convergence to Steady State of the Navier-Stokes Equations. *Journal of Computational Physics*, Vol 231, pp. 4867-4884.

[10] Hellsten, A. 2005. New Advanced k-omega Turbulence Model for High-Lift Aerodynamics. *AIAA Journal*, Vol. 43, No. 9, pp. 1857-1869, https://doi.org/10.2514/1.13754.

[11] Wallin, S. and Johansson, A. V. 2000. An Explicit Algebraic Reynolds Stress Model for Incompressible and Compressible Turbulent Flows. *J. Fluid Mechanics*, Vol. 403, 2000, pp. 89-132, https://doi.org/10.1017/S0022112099007004.

[12] Spalart, P. R. and Allmaras, S. R. 1994. A One-Equation Turbulence Model for Aerodynamic Flows. *Recherche Aerospatiale*, No. 1, pp. 5-21.

[13] Lötstedt, P. 1995. Accuracy of a propeller model in inviscid flow. *Journal of Aircraft*, vol. 32, No. 6.

[14] Rung, T., Lübcke, H. and Thiele, F. 2000. Universal wall-boundary conditions for turbulence-transport models. *ZAMM* 81(1), 1756–1758.

[15] Palombo, C. L. 2021. Development and validation of an improved wall-function boundary condition for computational aerodynamics. Master thesis, KTH, Engineering Mechanics.

[16] Perraud, J., Arnal, D., Casalis, G., Archambaud, J., and Donelli, R. 2009. Automatic transition predictions using simplified methods. AIAA J., Vol. 47, pp. 2676–2684.

[17] Amoignon, O., Pralits, J., Hanifi, A., Berggren, M. and Henningson, D. 2006. Shape Optimization for Delay of Laminar-Turbulent Transition. AIAA J. Vol. 44, No. 5. https://doi.org/10.2514/1.12431